NJC

PAPER

Cite this: *New J. Chem.*, 2019, **43**, 1459

A unified model of impact sensitivity of metal azides†

Sergey V. Bondarchuk

Received 12th September 2018,
Accepted 11th December 2018

DOI: 10.1039/c8nj04658a

rsc.li/njc

A comprehensive theoretical study of 18 metal azides is reported. Herein, the first theoretical model of impact sensitivity is developed which can safely distinguish sensitive and insensitive (alkali) metal azides. The model includes four solid-state criteria and three features of isolated atoms and molecules. Using ten azides with experimentally known crystal structures, we obtained the values of sensitivity function Ω which correlates well (R^2 = 0.91) with experimental impact energies. When three azides with a predicted crystal structure are added, the correlation becomes slightly poorer (R^2 = 0.84), but it still predicts alkali metal azides to be insensitive. Thus, the impact energies for sensitive azides lie in the range of 1–16 N cm^{-2}, while the predicted values for alkali metal azides lie in the range of 40–87 N cm^{-2}. Theoretical background for the proposed model of impact sensitivity is discussed in the paper.

Introduction

Despite the fact that a huge body of literature is dedicated to the problem of impact sensitivity, this phenomenon still remains to be a serious challenge for theorist who work in the field of high-energy density materials (HEDMs). Recent interest in the nitrogen-rich HEDMs including both the covalently bound[1–4] and molecular[5,6] crystalline materials requires a somewhat different approach for quantifying impact sensitivity than that based on the estimation of the molecular features.[7–11] Often, a simple look of a skilled chemist at a molecular structure of a HEDM can provide some insight into the degree of its impact sensitivity. Thus, analyzing the structure of a HEDM, one should pay attention to the presence of: (i) strong electron-withdrawing groups (NO_2, ONO_2, $NHNO_2$, $N(NO_2)_2$, *etc.*); (ii) strained cycles, bonds, and cages; (iii) localization or delocalization of the electron charge; (iv) intramolecular hydrogen bonding; (v) resonance stabilization, and so forth. No doubt, the presence of the above-mentioned structural factors should destabilize the molecule and, as a result, make it more sensitive to impact loadings or any other external energetic perturbations. But what can we say about the mechanism underlying impact sensitivity and what is the role of structural factors? This puzzle remains to be unsolved.

One of the main problems of the molecular approach in studying impact sensitivity is that the real samples are solid crystalline materials, not isolated molecules in a vacuum. Therefore, a number of very important properties cannot be taken into account since these are the features of solid state only. Of course, the molecular properties, like bond dissociation energies or topological parameters, and the presence of explosophores affect impact sensitivity more than the crystalline parameters do. But the calculations of an isolated molecule are reasonable only for molecular crystals, when a molecule can serve as a representative of the whole material. In the case of ionic systems (metal azides), the calculation of crystals is the only way towards a physically reasonable modeling of the substance. Moreover, the presence of defects, like impurities or voids, will also affect impact sensitivity, but these factors have mainly stochastic nature and cannot be unambiguously estimated within first-principles calculations of crystals.

Thus, a natural drawback of the molecular approach is polymorphism of crystals. It is known that different crystalline forms of hexahydro-1,3,5-trinitro-1,3,5-triazine (RDX) and octahydro-1,3,5,7-tetranitro-1,3,5,7-tetrazocine (HMX) have different impact sensitivity.[12–15] Another example of such drawbacks is impact sensitivity of phenyl diazonium chloride and tetrafluoroborate, which have the same organic fragment and differ only in the nature of the anions. Recently, we have rationalized their different response to impact by the values of metallization point and stored energy content.[16] Zhu and Xiao proposed earlier that the band gap of an explosive can serve as a criterion of impact sensitivity.[17–19] Indeed, the electron occupation of the conduction band can lead to bond breaking and the corresponding formation of free radicals or other reactive species, since the virtual orbitals forming the conduction band usually have anti-bonding character with respect to most of the bonds.[20,21] But this oversimplified approach is scarcely applicable because the

Department of Chemistry and Nanomaterials Science, Bogdan Khmelnitsky Cherkasy National University, blvd. Shevchenko 81, 18031 Cherkasy, Ukraine. E-mail: bondchem@cdu.edu.ua

† Electronic supplementary information (ESI) available: Structural data, Brillouin zones, partial densities of states, calculated elastic stiffness constants, graphical presentation of the Young moduli and the frontier orbital energies. See DOI: 10.1039/c8nj04658a

values of the band gaps are generally too high to allow an effective thermal occupation of the conduction band.

It is well known, however, that crystal compression results in closure of the band gap. This occurs when the concentration of matrix atoms reaches a critical value given by the theories of Herzfeld, Mott, Hubbard, Edwards, Sienko and others.[22] On the other hand, decreasing of the band gap yields increased sensitivity according to the principle of the easiest transition of electrons (PET).[23] Thus, the effect of hydrostatic compression on the electronic properties of 2-diazo-4,6-dinitrophenol (DDNP),[24] RDX,[25] HMX,[14,26] 1,3,5-triamino-2,4,6-trinitrobenzene (TATB)[27,28] and nitromethane (CH_3NO_2)[29] has the same nature and leads to narrowing of the band gap. Zhu and Xiao reported, however, that the band gap can demonstrate flat regions (AgN_3)[30] or even increase (NH_4ClO_4)[31] with increased external pressure. In our recent study of a series of C–H–N–O–Cl explosives, we have found that the response of the band gap to hydrostatic compression has generally linear character with different slopes.[32] The latter determines the so-called band gap compressibility (β_E), which is particular for each single explosive, eqn (1).[32]

$$\frac{1}{\beta_E} = \left(\frac{P_{metal}}{\Delta E_{gap}}\right) = \tan\alpha, \quad (1)$$

where P_{metal} (GPa) is the value of external pressure corresponding to ΔE_{gap} = 0 eV (metallic state).

In the general case, it is not necessary to compress the crystal up to the metallic state, since at 298 K, a noticeable thermal occupation of the conduction band starts when the band gap is decreased at least to 1 eV.[33,34] Thus, instead of the metallization point, one should find the so-called triggering pressure (P_{trigg}), which corresponds to the 1 eV band gap in a solid.[32] Computationally, this procedure is rather expensive, since the β_E is unknown; as a result, a few trials are mandatory to search for a P_{trigg} value. In the present report, we have tried to replace the band gap compressibility with the crystal compressibility (β) or bulk modulus ($B = 1/\beta$). Indeed, it was proposed earlier that the position of the metallization point (assuming the P_{trigg} values too) depends on the mechanical properties of a crystal.[22] For example, in a covalently-bound solid, which possesses sp^3 hybrid orbitals (like diamond), the energy W needed to close the gap can be expressed as the following eqn (2):[22]

$$W = k_\theta/4, \quad (2)$$

The force constant k_θ is then found as in eqn (3):

$$k_\theta = \frac{3l^3}{8}(C_{11} - C_{12}), \quad (3)$$

where l is the bond length (Å); C_{11} and C_{12} are the corresponding elastic stiffness constants (GPa). An analoguous analytical expression for the low-symmetry molecular or ionic crystals is expected to be very complex. Nevertheless, a correlation should exist between the crystal compressibility and the triggering pressure.

To check this hypothesis, we have studied structural, electronic and mechanical properties of 18 sensitive and insensitive metal azides with experimentally known as well as predicted in this work crystal structures; many of these species are well-known primary explosives.[35] The choice of these materials was inspired by the fact that metal azides were extensively studied both experimentally[36–43] and theoretically[44–49] and particular attention was paid to the band structure calculations and correlation of the band gap values with impact sensitivity (see, for example, review ref. 19). On the other hand, to the best of our knowledge, a unified theoretical model of impact sensitivity being able to distinguish sensitive and insensitive metal azides was not reported so far.

Computational details

The calculations presented herein were performed in terms of density functional theory (DFT)[50] within the generalized gradient approximation (GGA). All the calculations were carried out with Cambridge Serial Total Energy Package (CASTEP) code[51] as implemented in the Materials Studio 7.0 suite of programs.[52] Norm-conserving pseudopotentials (NCP)[53] have been applied during the calculations, which provides the lattice parameters being much closer to the experimental ones, especially compared with those obtained using ultrasoft pseudopotentials (USP).[54] Within this formalism, the states N-$2s^22p^3$, Cu-$3d^{10}4s^1$, Pb-$5s^25p^65d^{10}6s^26p^2$, Hg-$5d^{10}6s^2$, Ba-$5s^25p^66s^2$, Sr-$4s^24p^65s^2$, Ca-$3s^23p^64s^2$, Ag-$4s^24p^65s^14d^{10}$, Tl-$6s^25d^{10}6p^1$, Ni-$3s^23p^64s^23d^8$, Co-$4s^23d^7$, Mn-$4s^23d^5$, Cs-$5s^25p^66s^1$, Rb-$4s^24p^65s^1$, K-$3s^23p^64s^1$, Na-$2s^22p^63s^1$ and Li-$2s^1$ were treated as the valence electrons. The exchange–correlation functional due to Perdew–Burke–Ernzerhof (PBE)[55] was applied entirely. In the case of α-NaN_3, the band structure calculations were also performed using a hybrid functional HSE06.[56] For the GGA/PBE approach, the long-range effects have been taken into account using the Grimme form of the damped C_6 term.[57] The following extra parameters of van der Waals force field have been applied: Pb (C_6 = 654.6280 eV Å^6, R_0 = 1.9440 Å), Hg (C_6 = 594.5360 eV Å^6, R_0 = 1.7580 Å), Ba (C_6 = 2352.6270 eV Å^6, R_0 = 1.7620 Å), Tl (C_6 = 593.3959 eV Å^6, R_0 = 1.9890 Å) and Cs (C_6 = 3267.5951 eV Å^6, R_0 = 1.8020 Å).

The electronic wave functions were obtained by the density-mixing scheme[58] (for PBE) and preconditioned conjugate gradients method (for HSE06).[59] Thereafter, these were expanded in a plane wave basis set with an energy cutoff equal to 900 eV (66.1 Ry) for the cell relaxations and elastic constant calculations and 1000 eV (73.5 Ry) for band structure calculations. The finite basis set correction was also included entirely. Optimizations of the asymmetric cells were performed by means of the Broyden, Fletcher, Goldfarb and Shannon (BFGS) method.[60] Sampling of the Brillouin zone was performed using k-point grids generated by the Monkhorst–Pack algorithm. Separation of k-points was set to be 0.08 Å^{-1} for cell optimizations and elastic constant calculations and 0.05 Å^{-1} for all the rest of the calculations. Convergence criteria of the total energy were specified to 5×10^{-6} eV atom^{-1} in the SCF calculations and 1×10^{-6} eV atom^{-1} during the fixed geometry calculations.

The remaining convergence quality parameters are the following: force (0.01 eV Å^{-1}), stress (0.02 GPa) and displacement (5×10^{-4} Å).

Crystal habits were obtained using the attachment energy method[61] on the basis of crystal graph calculations with maximum Miller indices (3 3 3). The calculations of energy content, chemical hardness and electron affinities were based on energies obtained with the DMol^3 code[62] as part of the Materials Studio 7.0 program suite.[52] This allows calculations of both the isolated species and periodic solids to be performed within the same approach. Thus, we have applied all electron calculations with the PBE/DND (for energy content) and B3LYP/DND (for chemical hardness and electron affinity) approach including scalar relativistic effects.[62,63]

Results and discussion

Theoretical background

Recently, we have introduced a dimensionless sensitivity function Ω, which is proportional to impact energy or the h_{50} values.[32] This function is expressed by an empirical model comprising four complementary solid-state criteria of impact sensitivity, namely, triggering pressure, average number of electrons per atom N_F (atom^{-1}), crystal habit sphericity (Ψ), energy content (E_c, kJ mol^{-1} atom^{-1}) and melting point (T_m, K) eqn (4).[32]

$$\Omega = \frac{\Psi {T_m}^2}{{N_F}^7} \exp\left(\frac{P_{trigg}}{1000}\right) \exp\left(-\frac{E_c}{100}\right) \quad (4)$$

The Ψ quantity can be expressed as the following eqn (5).

$$\Psi = \frac{S_{cryst}}{6^{2/3} {V_{cryst}}^{2/3} \pi^{1/3}} \quad (5)$$

where S_{cryst} (Å^2) and V_{cryst} (Å^3) are the surface and volume of a crystal habit obtained by means of the crystal growth morphology calculations.

The crucial point in the proposed theoretical model is the thermally induced electron transfer from the valence to a conduction band. In contrast to the gaseous and liquid-phase reactions, where the formation of the excited triplet states can be promoted by an external perturbation (*e.g.*, paramagnetic species),[33] in solids, the formula units are fixed at the equilibrium positions and the molecular motion is restricted only by small displacements. Therefore, zero-pressure band structures of molecular crystals usually demonstrate flat bands assuming a weak intermolecular interaction. At high pressures, this interaction becomes stronger and the bands appear more curved. Thus, since the compression of a crystal causes simultaneous decreasing of the band gap and increasing of the temperature due to the plastic deformation and friction, the thermal electron occupation of the conduction band becomes possible.

The role of electronic excitations in initiation and propagation of detonation waves in solids was proposed by Williams in 1971.[64] Wu *et al.*[27] proposed that an indicator of metallization is the size of the band gap at typical detonation pressures. We have found, however, that detonation pressures of most explosives reduce the band gap approximately to 1 eV,[32] but as we have mentioned above, such gap is enough to allow the thermal electron transition. But how can an impact loading compress a crystal to such high pressures? To answer this question, one needs to consider this process at a microscopic level. Normally, the hammer surface is not ideally flat. As a result, only small restricted areas (contact zones) of the hammer surface first penetrate the explosive sample. This yields huge pressures, which can be comparable with the typical detonation pressures of common explosives and even higher.

It becomes clear that hard crystals require a stronger compression than soft ones. Thus, the crystal compressibility or the bulk moduli should also correlate with impact sensitivity. Such considerations agree with the tribochemical mechanism of initiation proposed by Fox in 1970, who studied thermal decomposition kinetics of single crystals of metal azides.[42] This assumes that the decomposition reaction can be initiated by a release of elastic strain energy when a fast crack runs through the material.[42] Thus, we assume that bulk moduli are directly proportional to impact energy.

Since the studied azides differ only in the nature of the metal cation, it is important to account energetic parameters of the cation reactivity. In a vacuum, the decomposition reaction of metal azides can be written as the following:

$$M^{n+}(N_3^-)_n \rightarrow M + 3n/2N_2$$

Obviously, reduction of cations first yields metal atoms, which then form nanoclusters and, finally, form nuclei. Therefore, for the calculation the E_c values, we have applied energies of isolated states of metals. Moreover, electron affinities (A) of the metal cations are the good descriptors of the reduction process, which should be inversely proportional to the impact energy. Herein, we define A as the difference between M^{n+} and M^0 states.

Finally, the values of chemical hardness (η) are included in the developed model of impact sensitivity. Indeed, according to the known ''principle of maximum hardness'', the intrinsic driving force of the reaction is determined by the change in chemical hardness between products and reactants.[65] In other words, formation of the hardest species is the most preferable reaction. Taking into account Koopmans' theorem, the quantity η can be expressed as in eqn (6):[65]

$$\eta = I - A = -E_{HOMO} + E_{LUMO} \quad (6)$$

where I and A are ionization energy and electron affinity (in eV); E_{HOMO} and E_{LUMO} are the energies of the highest occupied and the lowest unoccupied molecular orbital, respectively. Thus, it is obvious that the η values should be directly proportional to the impact energy.

Computational support

The experimental and calculated lattice parameters of the studied metal azides are listed in Table 1 and the asymmetric cells along with atomic charges and bond lengths are illustrated in Fig. 1. As it follows from Table 1, the calculated structural parameters are rather close to the experimental ones. Relative error (δ) of the unit cell volume estimation does not

Table 1 The calculated (GGA/NCP/PBE-Grimme) and experimental (in parentheses) asymmetric cell parameters of the studied metal azides

Azide	a (Å)	b (Å)	c (Å)	β (°)	Ref.
$Cu(N_3)_2$	8.885 (9.084)	12.398 (13.454)	3.313 (3.079)		40
CuN_3	8.221 (8.653)		5.953 (5.594)		43
α-$Pb(N_3)_2$	6.443 (6.630)	16.419 (16.250)	11.278 (11.310)		41
$Hg_2(N_3)_2$	5.695 (5.961)	13.011 (12.591)	3.556 (3.580)	100.87 (103.25)	66
α-$Hg(N_3)_2$	10.865 (10.632)	6.148 (6.264)	6.220 (6.323)		39
$Ba(N_3)_2$	9.719 (9.590)	4.158 (4.390)	5.465 (5.420)	100.00 (99.75)	67
$Sr(N_3)_2$	11.739 (11.820)	11.690 (11.470)	6.129 (6.080)		68
$Ca(N_3)_2$	11.400 (11.338)	11.211 (11.038)	5.940 (5.938)		68
AgN_3	5.370 (5.617)	6.170 (5.915)	6.340 (6.006)		69
TlN_3	6.131 (6.208)		7.591 (6.208)		36
α-CsN_3	6.425 (6.541)		7.988 (8.091)		36
α-RbN_3	6.233 (6.310)		7.543 (7.519)		36
KN_3	6.111 (6.113)		7.023 (7.094)		36
α-NaN_3	6.163 (6.211)	3.731 (3.658)	5.143 (5.323)	103.12 (108.43)	38
LiN_3	5.602 (5.627)	3.282 (3.319)	4.854 (4.979)	104.06 (107.40)	38

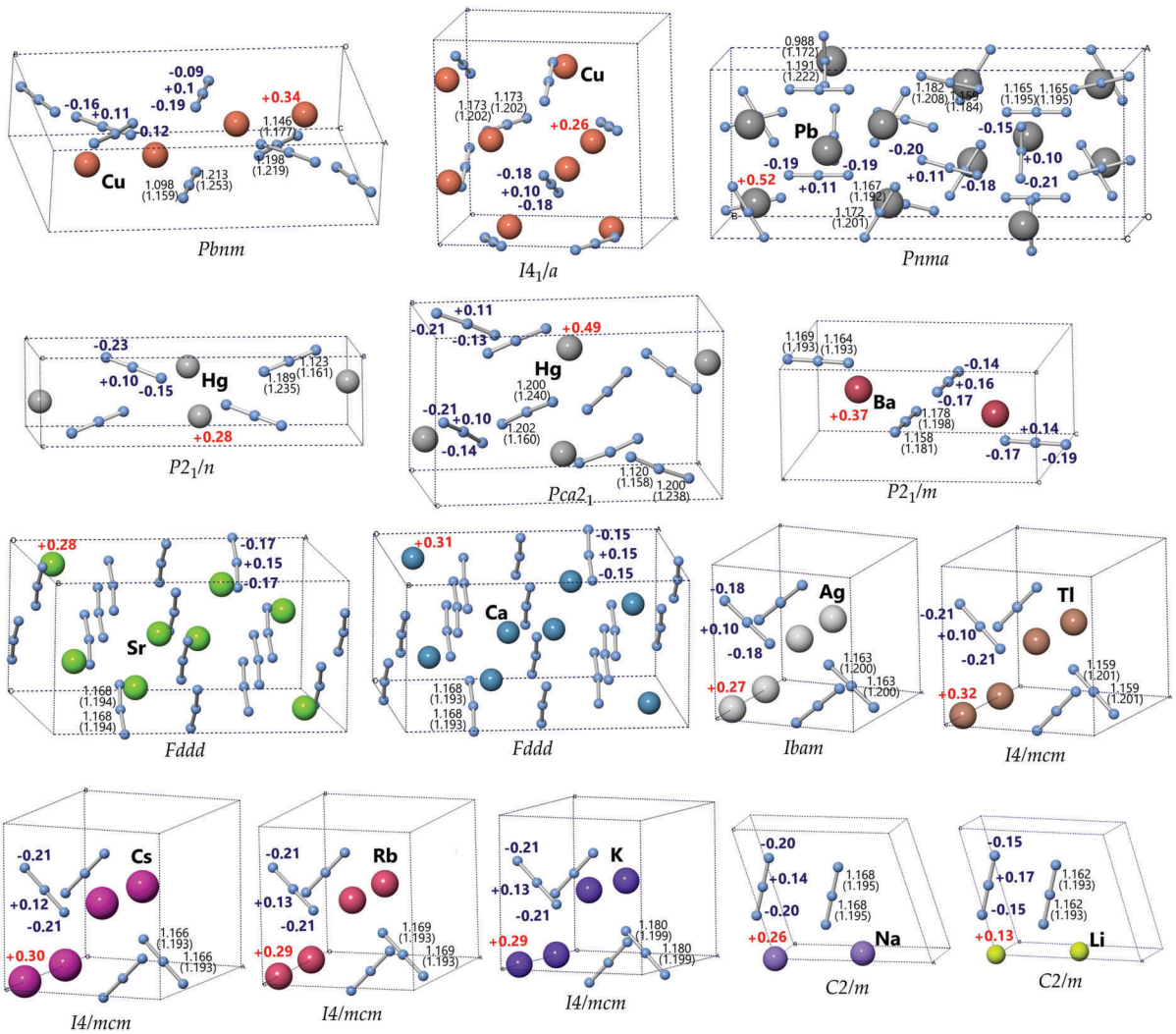

Fig. 1 Asymmetric cells of the studied metal azides. The symmetry unique numerical data include: Hirshfeld charges (in a.u.) and the N–N bond lengths (in Å).

exceed ±5% and the average value is −1% (Table S1 in the ESI†). Although, since the use of the GGA/NCP/PBE-Grimme approach is rather computationally expensive, we have tried to find a suitable, but less expensive method. For this purpose we have applied GGA/USP/PBE-Grimme and GGA/USP/PW91 methods; the latter was used earlier by Zhu *et al.*[46,48] and the

reported structural results appeared to be very close to the experimental ones. The results of our calculations of 6 azides are gathered in Table S2 in the ESI.† As one can see in Table S2 (ESI†), the δ values of Zhu *et al.*[46,48] are much lower than ones obtained in this work. Actually, we cannot explain this mismatch, but we tend to trust our results. Anyway, for some azides, the δ values are too big to justify using USPs in this case. Thus, all the remaining calculations were performed using the GGA/NCP/PBE-Grimme approach.

Cartwright and Wilkinson[44] tried to correlate the minimum non-bonded N–N distances with impact sensitivity. Using the experimental data on impact energy for 6 azides, they obtained a rather good correlation with R^2 = 0.83;[44] however, this correlation cannot predict insensitivity for alkali metal azides. The same correlations with the N═N bond lengths, first and second ionization potentials, enthalpies of formation and lattice energies completely failed.[44]

Let us consider the band structures. The hypothesis about the role of band gap width in impact sensitivity of explosives was put forward long ago (see, for example, review ref. 19). According to this hypothesis, sensitive explosives must have small band gaps. But how can band gaps influence impact sensitivity? Obviously, one needs to talk about the role of excited states in the crystal decomposition and subsequent release of chemically aggressive radical, ionic or other species. From this point of view, zero-pressure band gaps are less important since these are too wide to be effectively occupied under simple thermal excitation.

The calculated values of ΔE_{gap} along with the available experimental data are presented in Table 2 and the corresponding band structure plots are illustrated in Fig. 2. As one can see in Table 2, alkali metal azides demonstrate huge gaps 8–9 eV and even sensitive α-$Pb(N_3)_2$ has ΔE_{gap} = 3.5 eV. The calculated values are about two times lower than the corresponding experimental gaps. This is the known problem of band gap underestimation by pure GGA functionals, like PBE. Recently, we have demonstrated that hybrid functionals PBE0, B3LYP and HSE06 provide ΔE_{gap} approximately 1–1.5 eV higher

Table 2 Electronic properties of the studied metal azides

Azide	ΔE_{gap}	VBM[b]	CBM[c]	$\Delta E_{gap}{}'$[a]	Ref.
$Cu(N_3)_2$	2.544	*Γ*	*T*		
CuN_3	1.377	*Γ*	*Γ*		
α-$Pb(N_3)_2$	2.424	*Γ*	*Y*	3.50	70
$Hg_2(N_3)_2$	2.275	*Y*	*C*		
α-$Hg(N_3)_2$	3.002	*Y*	*X*		
$Ba(N_3)_2$	3.588	*Γ*	*Γ*	7.00	71
$Sr(N_3)_2$	3.689	*X*	*Γ*	7.00	71
$Ca(N_3)_2$	3.500	*X*	*Γ*		
AgN_3	1.329	*T*	*Z*	3.50	72
TlN_3	1.846	*Z*	*X*		
α-CsN_3	3.622	*Z*	*Z*	8.61	73
α-RbN_3	3.705	*Z*	*Z*	8.82	73
KN_3	4.036	*Z*	*Z*	8.55	73
α-NaN_3	4.028	*Z*	*L*	8.46	73
LiN_3	3.667	*Z*	*L*		

[a] Experimental value. [b] Valence band maximum. [c] Conduction band minimum.

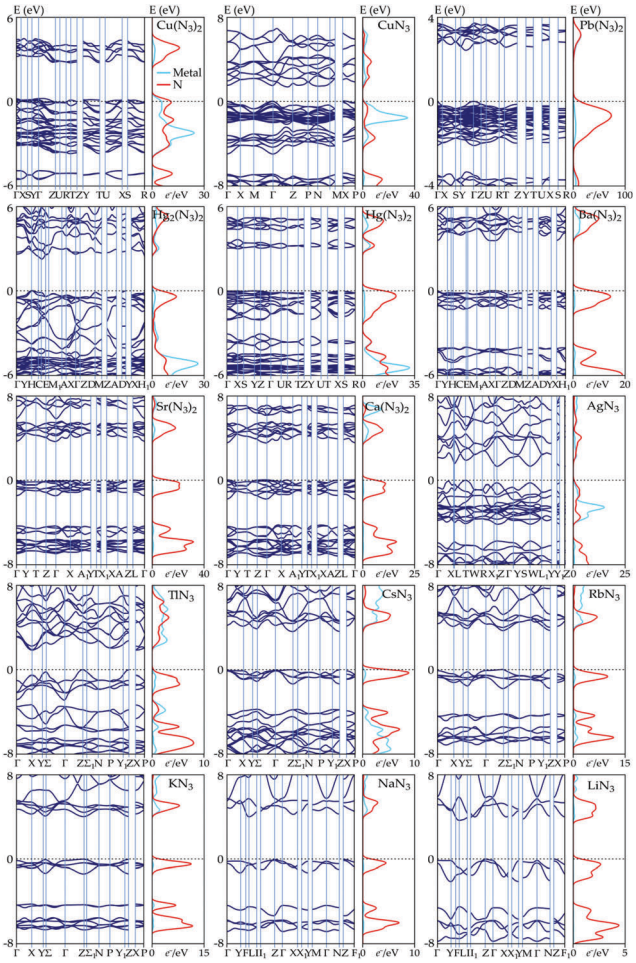

Fig. 2 Band structure and partial density of states (PDOS) of the studied metal azides.

than the ones obtained with pure functionals.[1,74] Thus, we have calculated a band structure for α-NaN_3 using the GGA/HSE06 approach and obtained the ΔE_{gap} = 5.207 eV, which is still too far from the experimental value of 8.46 eV (Table 2).

On the other hand, the calculated ΔE_{gap} values correlate well (R^2 = 0.83) with the experimental data (Table 2). The corresponding regression equation has the following form: $\Delta E_{gap}{}' = 2.1564\Delta E_{gap} - 0.1917$. Therefore, since the same trend is observed, the calculated values of the band gaps can be safely used for correlation with impact energies. It is worth noting that integration of the Brillouin zones (BZ) for band structure calculations was performed in accordance with the high-throughput approach which offers the standard integration paths for all the 24 BZ.[75] Positions of the high-symmetry points in the BZ of the studied metal azides are presented in Fig. S1 and the element contributions in partial density of states are illustrated in Fig. S2 in the ESI.†

Meanwhile, as we have shown earlier, the value of 1 eV is the energetic boundary between thermal and photochemical reactions.[33] Though, it does not mean that an effective thermal electron occupation of the conduction band should take place when the band gap is close to 1 eV. According to the

Boltzmann distribution, in this case the temperature must be high enough to start decomposition of many organic substances. This is the reason why CuN_3 (estimated $\Delta E_{gap}' = 2.778 \pm 1$ eV) is so thermally unstable. Moreover, CuN_3 exhibits a direct band gap $\Gamma \rightarrow \Gamma$ (Table 2), which allow an effective electron transition. Anyway, a simple correlation of zero-pressure ΔE_{gap} values with impact sensitivity parameters is rather speculative and does not reflect the mechanism of this phenomenon. For example, monoaminotrinitrobenzene (MATB) with h_{50} = 177 cm has ΔE_{gap} = 1.89 eV. Hexanitrohexaazaisowurtzitane (HNIW) has ΔE_{gap} = 3.63 eV and h_{50} = 27 cm (2.5 kg weight).[19] Probably, such inconsistency is due to different decomposition mechanisms for MATB (the so-called trinitrotoluene mechanism[76]) and HNIW (homolysis of the longest N–N bond). In any case, it is necessary to consider the factors leading to a decrease in the ΔE_{gap} values.

As we have mentioned in the previous section, elastic properties of a crystal should correlate with its impact sensitivity. Thus, we have replaced the band gap compressibility (β_E)[32] with the bulk modulus (B). For this purpose, we have calculated elastic properties of the studied metal azides including bulk (B, GPa) and shear (G, GPa) moduli, the isotropic value of Young modulus (E_{iso}, GPa) and the isotropic value of Poisson ratio (ν_{iso}); the results are listed in Table 3. Numerical values of independent elastic stiffness (C_{ij}) constants as well as 3D contours of the Young moduli are presented in Table S3 and Fig. S3 in the ESI.†

As it follows from Table 3, there is a good coincidence between the calculated and available experimental data on the B values. It is interesting that the latter correlate with impact energy values, except for TlN_3 with R^2 = 0.63. But such an oversimplified approach cannot explain why alkali metal azides are insensitive, since the B value for LiN_3 is lower than for all the sensitive azides, except for $Cu(N_3)_2$ and $Hg(N_3)_2$ (Table 3). The other elasticity parameters in Table 3 demonstrate the absence of the correlation with impact energy.

Another criterion considered in this work is crystal habit sphericity Ψ (eqn (5)). This parameter is proportional to the amount of free space between distinct crystals in a sample. For an effective compression caused by an impact loading, the crystals should be placed as tight as possible. Since the most tightly packed particles are ideal spheres with Ψ = 1, and for real crystal habits $\Psi > 1$, this parameter should be directly proportional to the applied impact energy. Thus, the calculated values of Ψ are listed in Table 4 and the vacuum morphology of the crystal habits is illustrated in Fig. 3. Of course, one should keep in mind that the morphology depends on experimental conditions of the crystal growth which can distort the Ψ value. Therefore, to be more rigorous, solvent effects must be taken into account as it is done, for example, in terms of the modified attachment energy (MAE) method.[80]

The last solid-state property is the stored energy content E_c (Table 4). Recently, we have proposed to use E_c in an exponential

Table 3 The calculated elasticity parameters of the studied metal azides and experimental impact energies IE

Azide	IE (N cm^{-2})	B (GPa)	G (GPa)	E_{iso}	ν_{iso}
$Cu(N_3)_2$	1.50[a]	17.66	6.60	75.67	0.2397
CuN_3	2.66[b]	23.93	14.57	36.67	0.4333
α-$Pb(N_3)_2$	4.76[b]	36.38	42.03	92.65	0.1421
$Hg_2(N_3)_2$	4.76[b]	32.38	8.55	30.59	0.3281
α-$Hg(N_3)_2$	5.19[a]	17.07	8.86	24.72	0.2616
$Ba(N_3)_2$	7.70[b]	38.69	11.88	34.59	0.3653
$Sr(N_3)_2$	9.10[b]	40.92	17.96	45.69	0.3275
$Ca(N_3)_2$	10.14[b]	44.35	21.96	60.11	0.2898
AgN_3	6.82[b]	46.53	15.89	61.01	0.3219
TlN_3	16.18[b]	23.99	10.60	29.51	0.3228
α-CsN_3	Not explosive[b]	32.97	15.29	39.25	0.3318
α-RbN_3	Not explosive[b]	39.45	19.02	41.97	0.3270
KN_3	Not explosive[b]	27.73[c]	15.84	38.36	0.2835
α-NaN_3	Not explosive[b]	19.75[d]	10.26	28.88	0.2560
LiN_3	Not explosive[b]	18.43[e]	18.53	45.04	0.1069

[a] From ref. 35. [b] From ref. 44. [c] Experimental value 27.4 GPa.[77] [d] Experimental value 17.5 GPa.[78] [e] Experimental value 19.1 GPa.[79]

Table 4 The calculated atomic and molecular criteria along with the crystal habit sphericity

Azide	Ψ	E_c[a]	η[b]	A[b]	N_F[c]	Ω	IE′[d]
$Cu(N_3)_2$	1.248	44.09	8.933	30.345	5.86	3.501	3.15
CuN_3	1.131	26.34	4.300	8.040	6.50	27.017	4.77
α-$Pb(N_3)_2$	1.152	35.75	12.039	19.999	7.43	16.427	4.04
$Hg_2(N_3)_2$	1.204	27.52	2.459	10.247	6.75	13.190	3.82
α-$Hg(N_3)_2$	1.166	75.05	7.563	29.237	6.00	2.731	3.10
$Ba(N_3)_2$	1.239	3.44	19.574	14.679	5.71	76.213	8.17
$Sr(N_3)_2$	1.136	1.06	25.287	16.288	5.71	77.742	8.27
$Ca(N_3)_2$	1.302	15.62	31.161	17.562	5.71	100.873	9.87
AgN_3	1.106	15.40	6.469	7.567	8.50	67.443	7.56
TlN_3	1.245	24.67	9.728	4.621	7.00	189.998	16.02
α-CsN_3	1.252	−75.08	14.947	3.336	6.00	999.943	71.91
α-RbN_3	1.300	−53.24	17.667	3.748	6.00	1138.106	81.44
KN_3	1.245	−36.37	21.042	3.951	6.00	807.447	58.62
α-NaN_3	1.154	−42.54	32.853	4.943	6.00	535.058	39.83
LiN_3	1.162	−47.38	57.423	5.152	4.00	1218.596	86.99

[a] In kJ mol^{-1} atom^{-1}. [b] In eV. [c] In atom^{-1}. [d] In N cm^{-2}.

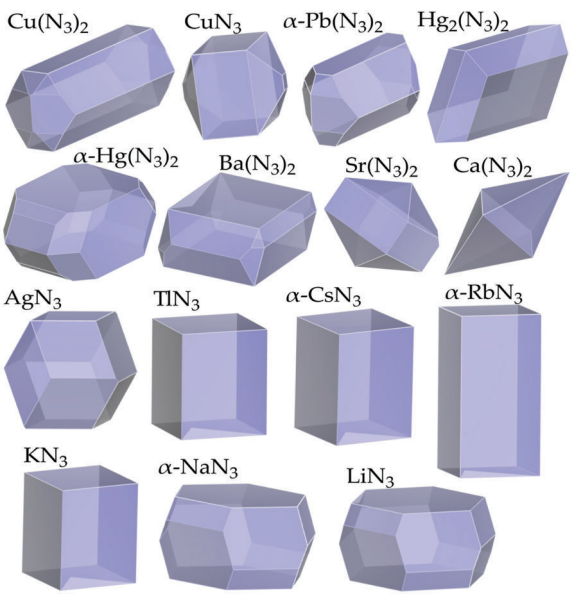

Fig. 3 The calculated growth morphology of the studied metal azide crystals in a vacuum.

form to avoid negative values.[32] Indeed, as one can see in Table 4, alkali metal azides have negative energy content meaning that their decomposition is endothermic. The remaining azides possess positive E_c values. Thus, this quantity safely distinguishes the sensitive and insensitive species. Herein, we should stress that the decomposition pattern for alkaline earth azides is somewhat different from those of the rest of the azides (described above). It is known that alkaline earth azides decompose to the corresponding nitrides in accordance with the following scheme:[44,81]

$$3M(N_3)_2 \rightarrow M_3N_2 + 8N_2, \quad \text{when M = Ca, Sr and Ba.}$$

Thus, we have used the completely relaxed asymmetric cells of these three nitrides (space group $Ia\bar{3}$) from the previous study[82] and calculated the corresponding E_c values (Table 4). Except for the values for $Hg(N_3)_2$ and TlN_3, a simple dependence between $\exp(-E_c/1000)$ and the experimental impact energies demonstrates rather good correlation coefficient (R^2 = 0.69).

Among the properties of isolated atoms and molecules we consider N_F, η and A quantities (Table 4); the corresponding values of HOMO and LUMO energies as well as the total energies of cationic and neutral states of metals are listed in Table S4 in the ESI.† The first of them is calculated as the sum of all "valence" electrons (see Computational details) in the molecule divided by the number of atoms. In other words, N_F corresponds to the total integrated density of states at the Fermi level normalized per atom. It is obvious that N_F is directly proportional to the probability of electron transitions in a crystal. Therefore, this quantity should be inversely proportional to the impact energy.

The latter two criteria, η and A, are the most informative in the present model, since trends of their change are tracked through all the azides. As it follows from Table 4, the η values increase and the A values decrease with increase of impact energy. Indeed, the decomposition of alkali metal azides assumes that extremely hard species, for example, the Li^+ cation, must be reduced to much softer ones (lithium atom). At the same time, the A values determine how much energy is released after reduction. This means that impact energy is directly proportional to η, but is inversely proportional to A.

Thus, combining all the above discussed criteria together, we have developed an empirical sensitivity function (Ω), which can be expressed as in eqn (7).

$$\Omega = \frac{B\Psi\eta}{N_F A^2}\exp\left(\frac{\Delta E_{gap} - E_c}{1000}\right) \quad (7)$$

The calculated values of Ω are listed in Table 4. On the basis of these values, we have obtained the following regression IE′ = 0.069Ω + 2.910, which provides correlation coefficient R^2 = 0.91. The predicted impact energies are listed in Table 4 and the plot of IE *versus* IE′ is illustrated in Fig. 4. Several statistical functions including standard deviation (SD), median (Me) and confidence interval at 99% probability are presented as the inset in Fig. 4. As it follows from Table 4, there is a wide energetic gap between sensitive and insensitive azides (at least *ca.* 24 N cm^{-2}).

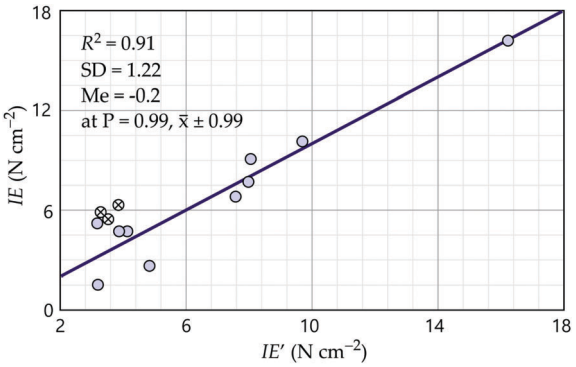

Fig. 4 Correlation between the predicted and experimental impact energies of the studied metal azides.

Three crosshair markers in Fig. 4 correspond to $Ni(N_3)_2$, $Co(N_3)_2$ and $Mn(N_3)_2$, for which the crystal structure is unknown, but experimental impact energies are available. In order to include these azides in the general correlation, we have predicted their crystal structures using a simulated annealing method, which assumes generation of a huge number of random crystal structures and subsequent search for the most stable regions on the potential energy hypersurface.[52]

The calculation has been started from a cubic unit cell with density 1.85 g cm^3 in the $P1$ space group symmetry. At the end of geometry optimization we have obtained a monoclinic crystal system of the $C2/m$ space group for all three azides. The asymmetric cells along with the corresponding band structure plots and predicted crystal growth morphology are presented in Fig. 5.

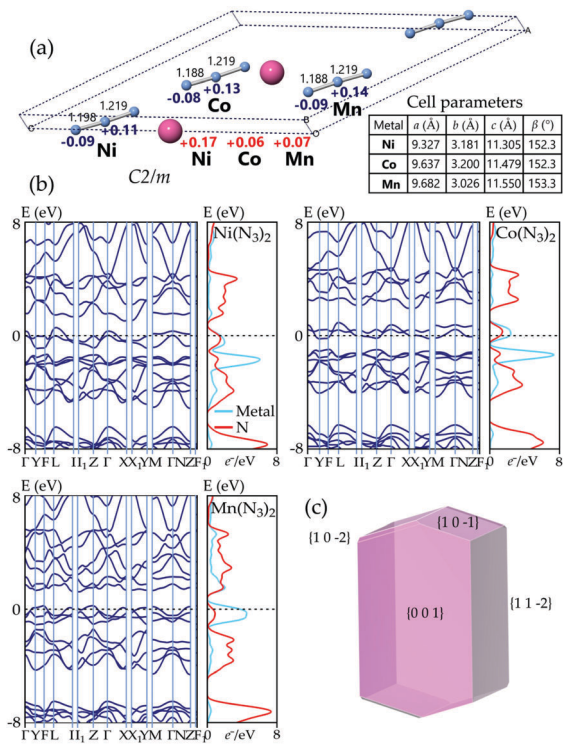

Fig. 5 The predicted crystal packing, band structure and growth morphology for $Ni(N_3)_2$, $Co(N_3)_2$ and $Mn(N_3)_2$.

Table 5 Parameters of impact sensitivity for three azides with predicted crystal structures

Criterion	$Ni(N_3)_2$	$Co(N_3)_2$	$Mn(N_3)_2$
Ψ	1.224	1.230	1.236
E_c [a]	70.71	56.60	46.64
η [b]	7.508	4.197	8.218
A [b]	23.759	25.107	23.265
N_F [c]	6.86	5.57	5.29
ΔE_{gap} [b]	0.478	1.005	1.030
B [d]	34.15	32.27	36.11
Ω	7.558	4.487	12.248
IE [e]	5.46[44]	5.88[44]	6.30[44]
IE′ [e]	3.43	3.22	3.75

[a] In kJ mol^{-1} $atom^{-1}$. [b] In eV. [c] In $atom^{-1}$. [d] In GPa. [e] In N cm^{-2}.

It is worth noting that the possible presence of more stable polymorphs as well as the dynamical stability of the crystals is neglected in such crystal structure prediction. This can distort results of the solid-state criteria calculations, but taking into account that Ψ and $\exp((\Delta E_{gap} - E_c)/1000)$ are both close to 1, the main factor of error is the value of bulk modulus. The calculated data together with the experimental impact energies for these three azides are gathered in Table 5. Thus, when three predicted points are included, the general correlation becomes slightly poorer (R^2 = 0.84), but it still applicable to distinguish sensitive and insensitive metal azides.

Conclusions

In summary, we have presented the first unified model of impact sensitivity of metal azides applying for 18 crystals, both sensitive and insensitive. The model comprises four solid-state criteria and three properties of isolated species. Application of the solid-state criteria is rationalized in terms of the previous theoretical considerations about the role of pressure induced thermal electron excitation in crystalline explosives.[32,83,84] These criteria seem to have general character and applicability. Meanwhile, energetic description of elementary stages of the decomposition reaction appeared to be crucial in the present model. Thus, the values of chemical hardness η and electron affinity A are the only criteria which regularly change from the most sensitive to insensitive azides.

The use of the abovementioned solid-state criteria was found to be rather successful for different families of C–H–N–O–Cl explosives including aromatic, aliphatic and heterocyclic nitro and nitrato compounds.[32] On the other hand, this methodology requires crystal structures to be determined, but this is quite problematic when modeling novel explosives, since it needs very computationally expensive crystal structure prediction. This is a probable reason why the predicted impact energies for $Ni(N_3)_2$, $Co(N_3)_2$ and $Mn(N_3)_2$ slightly decrease the R^2 value. Thus, a simple method for transformation of an isolated molecule to the condensed (crystalline) state is very desirable. But in the case of an unknown crystal structure, the melting temperature and crystal habit sphericity (Ψ) terms must be omitted.

We should stress, however, that the computational approach, which is described in the present paper, involve two suppositions. The first is that $\beta_E < 0$ and has a linear character. Secondly, the studied crystal does not demonstrate any phase transitions until ΔE_{gap} = 1 eV. Otherwise, one cannot correctly estimate β_E, and consequently the supposition that β_E is proportional to $1/B$ has no sense. Thus, applicability of the present theoretical approach to crystals, which demonstrate phase transitions or nonlinear behavior of band gap compressibility, requires a more detailed study in future.

Conflicts of interest

There are no conflicts to declare.

Acknowledgements

This work was supported by the Ministry of Education and Science of Ukraine, Research Funds (Grants No. 0117U003908 and 0118U003862).

Notes and references

1 S. V. Bondarchuk and B. F. Minaev, *Phys. Chem. Chem. Phys.*, 2017, **19**, 6698–6706.
2 S. V. Bondarchuk and B. F. Minaev, *Comput. Mater. Sci.*, 2017, **133**, 122–129.
3 S. V. Bondarchuk and B. F. Minaev, *Mol. Phys.*, 2017, **115**, 2423–2430.
4 M. I. Eremets, A. G. Gavriliuk, I. A. Trojan, D. A. Dzivenko and R. Boehler, *Nat. Mater.*, 2004, **3**, 558–563.
5 M. J. Greschner, M. Zhang, A. Majumdar, H. Liu, F. Peng, J. S. Tse and Y. Yao, *J. Phys. Chem. A*, 2016, **120**, 2920–2925.
6 B. Hirshberg, R. Benny Gerber and A. I. Krylov, *Nat. Chem.*, 2014, **6**, 652–656.
7 G. Fayet and P. Rotureau, *J. Loss Prev. Process Ind.*, 2014, **30**, 1–8.
8 G. Shuo, *Adv. Mater. Res.*, 2013, **641–642**, 109–112.
9 D. Mathieu and T. Alaime, *J. Mol. Graphics Modell.*, 2015, **62**, 81–86.
10 Z.-X. Chen and H.-M. Xiao, *Propellants, Explos., Pyrotech.*, 2014, **39**, 487–495.
11 Q.-L. Yan and S. Zeman, *Int. J. Quantum Chem.*, 2013, **113**, 1049–1061.
12 D. I. A. Millar, I. D. H. Oswald, D. J. Francis, W. J. Marshall, C. R. Pulham and A. S. Cumming, *Chem. Commun.*, 2009, 562–564.
13 A. J. Davidson, I. D. H. Oswald, D. J. Francis, A. R. Lennie, W. J. Marshall, D. I. A. Millar, C. R. Pulham, J. E. Warren and A. S. Cumming, *CrystEngComm*, 2008, **10**, 162–165.
14 Q. Peng, Rahul, G. Wang, G.-R. Liu and S. De, *Phys. Chem. Chem. Phys.*, 2014, **16**, 19972–19983.
15 K. L. McNesby and C. S. Coffey, *J. Phys. Chem. B*, 1997, **101**, 3097–3104.
16 S. V. Bondarchuk, *Int. J. Quantum Chem.*, 2017, **117**, e25430.
17 W. Zhu, X. Zhang, T. Wei and H. Xiao, *J. Mol. Struct. THEOCHEM*, 2009, **900**, 84–89.

18 H. Zhang, F. Cheung, F. Zhao and X.-L. Cheng, *Int. J. Quantum Chem.*, 2009, **109**, 1547–1552.
19 W. Zhu and H. Xiao, *Struct. Chem.*, 2010, **21**, 657–665.
20 S. V. Bondarchuk and B. F. Minaev, *J. Mol. Struct. THEOCHEM*, 2010, **952**, 1–7.
21 B. F. Minaev, S. V. Bondarchuk and M. A. Girţu, *J. Mol. Struct. THEOCHEM*, 2009, **904**, 14–20.
22 J. J. Gilman, *Philos. Mag. B*, 1993, **67**, 207–214.
23 H. M. Xiao and Y. F. Li, *Sci. China, Ser. B: Chem.*, 1995, **38**, 538–545.
24 Y. Liu, X. Gong, L. Wang and G. Wang, *J. Phys. Chem. C*, 2011, **115**, 11738–11748.
25 M. M. Kuklja and A. B. Kunz, *J. Appl. Phys.*, 1999, **86**, 4428–4434.
26 W. H. Zhu, X. W. Zhang, T. Wei and H. M. Xiao, *Theor. Chem. Acc.*, 2009, **124**, 179–186.
27 C. J. Wu, L. H. Yang and L. E. Fried, *Phys. Rev. B: Condens. Matter Mater. Phys.*, 2003, **67**, 235101.
28 Y. Kohno, K. Mori, R. I. Hiyoshi, O. Takahashi and K. Ueda, *Chem. Phys.*, 2016, **472**, 163–172.
29 E. J. Reed, J. D. Joannopoulos and L. E. Fried, *Phys. Rev. B: Condens. Matter Mater. Phys.*, 2000, **62**, 16500.
30 W. H. Zhu and H. M. Xiao, *J. Solid State Chem.*, 2007, **180**, 3521–3528.
31 W. H. Zhu, X. W. Zhang, W. Zhu and H. M. Xiao, *Phys. Chem. Chem. Phys.*, 2008, **10**, 7318–7323.
32 S. V. Bondarchuk, *J. Phys. Chem. A*, 2018, **122**, 5455–5463.
33 S. V. Bondarchuk and B. F. Minaev, *RSC Adv.*, 2015, **5**, 11558–11569.
34 S. V. Bondarchuk and B. F. Minaev, *Chem. Phys. Lett.*, 2014, **607**, 75–80.
35 R. Matyáš and J. Pachman, Explosive properties of primary explosives, *Primary explosives*, Springer-Verlag, Berlin, 2013.
36 U. Müller, *Z. Anorg. Allg. Chem.*, 1972, **392**, 159–166.
37 C. S. Choi and E. Prince, *J. Chem. Phys.*, 1976, **64**, 4510–4516.
38 G. E. Pringle and D. E. Noakes, *Acta Crystallogr., Sect. B: Struct. Crystallogr. Cryst. Chem.*, 1968, **24**, 262–269.
39 U. Müller, *Z. Anorg. Allg. Chem.*, 1973, **399**, 183–192.
40 R. Söderquist, *Acta Crystallogr., Sect. B: Struct. Crystallogr. Cryst. Chem.*, 1968, **24**, 450–455.
41 C. S. Choi, E. Prince and W. L. Garrett, *Acta Crystallogr., Sect. B: Struct. Crystallogr. Cryst. Chem.*, 1977, **33**, 3536–3537.
42 P. G. Fox, *J. Solid State Chem.*, 1970, **2**, 491–502.
43 H. Wilsdorf, *Acta Crystallogr.*, 1948, **1**, 115–118.
44 M. Cartwright and J. Wilkinson, *Propellants, Explos., Pyrotech.*, 2010, **35**, 326–332.
45 A. A. Denisaev, I. G. Assovskii and A. A. Berlin, *Dokl. Phys. Chem.*, 2013, **453**, 261–263.
46 W. Zhu and H. Xiao, *J. Comput. Chem.*, 2008, **29**, 176–184.
47 W. Zhu, J. Xiao and H. Xiao, *Chem. Phys. Lett.*, 2006, **422**, 117–121.
48 W. Zhu, J. Xiao and H. Xiao, *J. Phys. Chem. B*, 2006, **110**, 9856–9862.
49 W. Zhu and H. Xiao, *J. Phys. Chem. B*, 2006, **110**, 18196–18203.
50 W. Kohn and L. J. Sham, *Phys. Rev. A: At., Mol., Opt. Phys.*, 1965, **140**, A1133–A1138.
51 S. J. Clark, M. D. Segall, C. J. Pickard, P. J. Hasnip, M. J. Probert, K. Refson and M. C. Payne, *Z. Kristallogr.*, 2005, **220**, 567–570.
52 *Materials Studio 7.0*, Accelrys Inc., San Diego, CA, 2013.
53 J. S. Lin, A. Qteish, M. C. Payne and V. Heine, *Phys. Rev. B: Condens. Matter Mater. Phys.*, 1993, **47**, 4174–4180.
54 D. Vanderbilt, *Phys. Rev. B: Condens. Matter Mater. Phys.*, 1990, **41**, 7892–7895.
55 J. P. Perdew, K. Burke and M. Ernzerhof, *Phys. Rev. Lett.*, 1996, **77**, 3865–3868.
56 J. Heyd and G. E. Scuseria, *J. Chem. Phys.*, 2004, **121**, 1187–1192.
57 S. Grimme, *J. Comput. Chem.*, 2006, **27**, 1787–1799.
58 G. Kresse and J. Furthmüller, *Phys. Rev. B: Condens. Matter Mater. Phys.*, 1996, **54**, 11169–11186.
59 M. C. Payne, M. P. Teter, D. C. Allan, T. A. Arias and J. D. Joannopoulos, *Rev. Mod. Phys.*, 1992, **64**, 1045–1097.
60 R. Fletcher, *Practical methods of optimization*, Wiley, New York, 1980, vol. 1.
61 R. Docherty, G. Clydesdale, K. J. Roberts and P. Bennema, *J. Phys. D: Appl. Phys.*, 1991, **24**, 89–99.
62 B. Delley, *J. Chem. Phys.*, 2000, **113**, 7756–7764.
63 D. D. Koelling and B. N. Harmon, *J. Phys. C: Solid State Phys.*, 1977, **10**, 3107–3114.
64 F. Williams, *Adv. Chem. Phys.*, 1971, **21**, 289–302.
65 R. G. Pearson, *Acc. Chem. Res.*, 1993, **26**, 250–255.
66 P. Nockemann, U. Cremer, U. Ruschewitz and G. Meyer, *Z. Anorg. Allg. Chem.*, 2003, **629**, 2079–2082.
67 C. S. Choi, *Acta Crystallogr., Sect. B: Struct. Crystallogr. Cryst. Chem.*, 1969, **25**, 2638–2644.
68 H. Krischner and G. Kelz, *Z. Anorg. Allg. Chem.*, 1982, **494**, 203–206.
69 H. E. Marr and R. H. Stanford Jr., *Acta Crystallogr.*, 1962, **15**, 1313–1314.
70 H. D. Fair, Jr. and A. C. Forsyth, *J. Phys. Chem. Solids*, 1969, **30**, 2559–2570.
71 S. K. Deb, *Trans. Faraday Soc.*, 1963, **59**, 1423–1428.
72 J. N. Mycock, V. R. Pai Verneker and C. S. Gorzynski, Jr., *Spectrochim. Acta*, 1967, **23A**, 2849–2853; S. K. Deb, *Trans. Faraday Soc.*, 1963, **59**, 1414–1422.
73 S. K. Deb, *Trans. Faraday Soc.*, 1963, **59**, 1414–1422.
74 S. V. Bondarchuk and B. F. Minaev, *New J. Chem.*, 2017, **41**, 13140–13148.
75 W. Setyawan and S. Curtarolo, *Comput. Mater. Sci.*, 2010, **49**, 299–312.
76 R. Varga and S. Zeman, *J. Hazard. Mater.*, 2006, **A132**, 165–170.
77 K. Ramesh Babu and G. Vaitheeswaran, *Solid State Sci.*, 2013, **23**, 17–25; H. Zhu, F. Zhang, C. Ji, D. Hou, J. Wu, T. Hannon and Y. Ma, *J. Appl. Phys.*, 2013, **113**, 033511.

78 H. Zhu, F. Zhang, C. Ji, D. Hou, J. Wu, T. Hannon and Y. Ma, *J. Appl. Phys.*, 2013, **113**, 033511.
79 S. A. Medvedev, I. A. Trojan, M. I. Eremets, T. Palasyuk, T. M. Klapötke and J. Evers, *J. Phys.: Condens. Matter*, 2009, **21**, 195404.
80 N. Liu, Y.-N. Li, S. Zeman, Y.-J. Shu, B.-Z. Wang, Y.-S. Zhou, Q.-L. Zhao and W.-L. Wang, *CrystEngComm*, 2016, **18**, 2843–2851.
81 F. P. Bowden and H. T. Williams, *Proc. R. Soc. London, Ser. A*, 1951, **208**, 176–188.
82 E. Orhan, S. Jobic, R. Brec, R. Marchand and J.-Y. Saillard, *J. Mater. Chem.*, 2002, **12**, 2475–2479.
83 A. A. L. Michalchuk, P. T. Fincham, P. Portius, C. R. Pulham and C. A. Morrison, *J. Phys. Chem. C*, 2018, **122**, 19395–19408.
84 S. V. Bondarchuk, *CrystEngComm*, 2018, **20**, 5718–5725.

